Supplementary materials

A water-stable terbium metal-organic framework with functionalized ligands for the detection of Fe^{3+}, $Cr_2O_7^{2-}$ ions in water and picric acid in seawater

Hai-Huan Yu, [a] Jia-Qi Chi, [b] Zhong-Min Su, [*b, c] Xiao Li, [*b, c] Jing Sun [b, c] Chen Zhou, [b, c] Xiao-Li Hu [b, c] Qun Liu [a]

a School of Materials Science and Engineering, Changchun University of Science and Technology, Changchun 130022, People's Republic of China
b School of Chemistry and Environmental Engineering, Changchun University of Science and Technology, Changchun, 130022, People's Republic of China
c Jilin Provincial Science and Technology Innovation Center of Optical Materials and Chemistry, Changchun University of Science and Technology, Changchun, 130022, People's Republic of China
[*] E-mail: zmsu@nenu.edu.cn; lix@cust.edu.cn

Contents

Single-crystal X-ray diffraction data for Tb-MOF-A were recorded on a Bruker Apex CCD II area-detector diffractometer with graphite monochromated Mo-Kα radiation (λ = 0.71073 Å) at 296(2) K. Absorption corrections were applied using the multi-scan technique. Their structures were solved by the direct methods of SHELXS-97 and refined by the full-matrix least-squares technique with the SHELXL-97 program.10 Non-hydrogen atoms were refined with anisotropic temperature parameters. The crystal data and structure refinement results of Tb-MOF-A is summarized in Table S1. The CCDC number of Tb-MOF-A is 1974695.

Experimental

Materials and methods

The ligands phen (1,10-phenanthroline), H_2tftba (2,3,5,6 tetrafluoroterephthalic acid) and $Tb(NO_3)_3 \cdot 6H_2O$ were purchased from Adamas. Other chemicals and organic solvent were commercially available sources of analytical grade and used without further purification. The C, H, and N elemental analyses were conducted on a PerkinElmer 2400CHN elemental analyzer. Thermogravimetric analysis (TGA) data was obtained by PerkinElmer TG-7 analyzer in the temperature range of 25-800 °C at a heating rate of 10 °C min^{-1} under a flow of N_2. The powders' X-ray diffraction (PXRD) patterns were obtained using a Siemens D5005 under experimental conditions with Cu Kα X-ray radiation from $5° < 2\theta < 50°$ at a sweep speed of 0.2 °C·× 2θ min^{-1}. Fourier transform infrared (FT-IR) spectra were recorded in the range 4000-400 cm^{-1} using KBr pellets on an Alpha Centaurt FT/IR spectrophotometer. The ultraviolet-visible light (UV-Vis) absorption spectra were performed on a UV-5500(PC) UV-vis Spectrophotometer. Luminescent emission spectra were gained from F-4500FL fluorescence spectrophotometer.

Luminescence Sensing Measurements.

The luminescence sensing experiments of Tb-MOF-A were manipulated at room temperature by adding 3.0 mg of powder sample into 2.0 mL deionized water of $M(NO_3)_x$ ($M = Al^{3+}$, Fe^{3+}, Mn^{2+}, Mg^{2+}, Ca^{2+}, Co^{2+}, Cu^{2+}, K^+ and Na^+) or KX (X= PO_4^{3-}, CO_3^{2-}, SO_4^{2-}, $Cr_2O_7^{2-}$, NO_3^-,Br^-, ClO_4^-, CN^-, AcO^- and F^-) at the same concentration (1 mM), and the sensing experiment of PA was performed in simulated seawater which was made of the following composition:[1] NaCl (27.9 g/L), KCl (1.4 g/L), $MgCl_2$ (2.8 g/L), NaBr (0.5 g/L) and 2.0 of $MgSO_4$ (2.0 g/L). Then the mixtures were ultrasonicated for 45 min to detect directly.

Table S1. Crystallographic data for MOF **1**

	Tb-MOF-A
Empirical formula	$C_{24}H_{10}F_6N_2O_7Tb$
Formula weight	701.31
Temperature/K	273.15
Crystal system	monoclinic
Space group	C2/c
a/Å	19.6366(9)
b/Å	21.2636(11)
c/Å	11.5383(6)
α/°	90
β/°	101.743(2)
γ/°	90
Volume/Å^3	4716.9(4)
Z	8
ρ_{calc}g/cm^3	1.975
μ/mm^{-1}	3.096
F(000)	2665.0
Crystal size/mm^3	0.24 × 0.22 × 0.2
Radiation	MoKα (λ = 0.71073)
2Θ range for data collection/	5.262 to 50.324
Index ranges	-22 ≤ h ≤ 23, -25 ≤ k ≤ 25, -13 ≤ l ≤ 13
Reflections collected	41601
Independent reflections	4213 [R_{int} = 0.0387, R_{sigma} = 0.0191]
Data/restraints/parameters	4213/1212/362
Goodness-of-fit on F^2	1.040
R_1[a] [I>=2σ (I)]	R_1[a] = 0.0292,
wR_2[b] [all data]	wR_2[b] = 0.0731
Largest diff. peak/hole / e Å^{-3}	1.10/-1.01

R_1[a]= Σ||F_o|-|F_c||/Σ|F_o|, wR_2[b] = [Σ[w(F_o^2-F_c^2)^2]/Σ[w(F_o^2)^2]]$^{1/2}$.

Table S2 Selected bond distances (Å) and angles (º) for MOF **1**.

Bond distances (Å)			
Tb1-O1[1]	2.346(3)	Tb1-O5[2]	2.362(3)
Tb1-O2	2.347(3)	Tb1-O7	2.359(3)
Tb1-O3	2.323(3)	Tb1-N1	2.598(4)
Tb1-O4[1]	2.435(3)	Tb1-N2	2.547(4)
Symmetry transformations used to generate equivalent atoms: [1]3/2-X, 1/2-Y, 1-Z;[2]+X, 1-Y,1/2+Z;[3] 1-X,+Y,1/2-Z			
Bond angles (˚)			
O1[1]-Tb1-O2	125.20(11)	O3-Tb1-O5[2]	141.54(11)
O1[1]-Tb1-O4[1]	75.49(11)	O3-Tb1-O7	140.10(11)
O1[1]-Tb1-O5[2]	142.76(11)	O3-Tb1-N1	73.10(12)
O1[1]-Tb1-O7	77.17(11)	O3-Tb1-N2	77.94(12)

O1[1]-Tb1-N1	74.61(12)	O4[1]-Tb1-N1	141.73(12)
O1[1]-Tb1-N2	135.04(12)	O4[1]-Tb1-N2	149.40(12)
O2-Tb1-O4[1]	82.69(11)	O5[2]-Tb1-O4[1]	76.16(11)
O2-Tb1-O5[2]	73.85(11)	O5[2]-Tb1-N1	116.84(12)
O2-Tb1-O7	145.35(11)	O5[2]-Tb1-N2	75.16(12)
O2-Tb1-N1	134.64(12)	O7-Tb1-O4[1]	78.04(12)
O2-Tb1-N2	79.30(13)	O7-Tb1-O5[2]	73.73(11)
O3-Tb1-O1[1]	74.78(11)	O7-Tb1-N1	72.49(12)
O3-Tb1-O2	74.54(11)	O7-Tb1-N2	103.74(13)
O3-Tb1-O4[1]	120.55(11)	N2-Tb1-N1	63.53(13)

Symmetry transformations used to generate equivalent atoms: [1]3/2-X, 1/2-Y,1-Z; [2]+X,1-Y,1/2+Z; [3]+X,1-Y,-1/2+Z; [4]1-X,+Y,1/2-Z

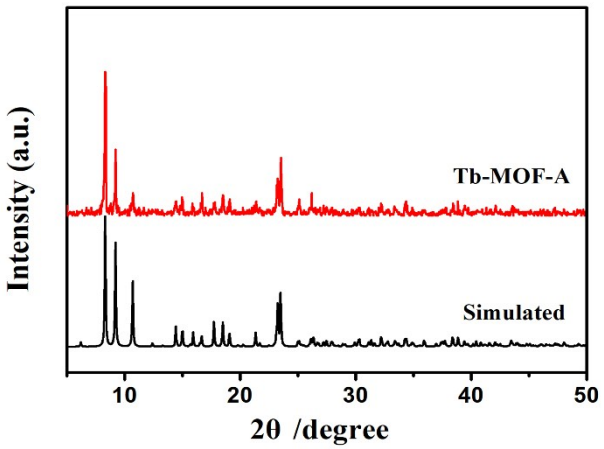

Figure S1 Experimental PXRD pattern of Tb-MOF-A and that simulated from the CIF file

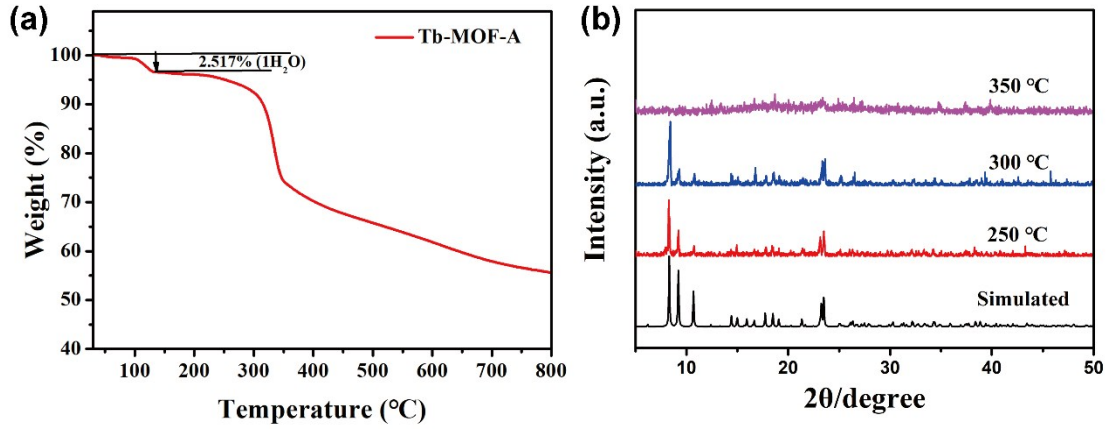

Figure S2 (a)Thermal gravimetric analyses (TGA) curve of Tb-MOF-A.(b) Simulated and experimental powder X-ray diffraction patterns (PXRD) patterns of Tb-MOF-A were heated at 250℃, 300℃, 350℃

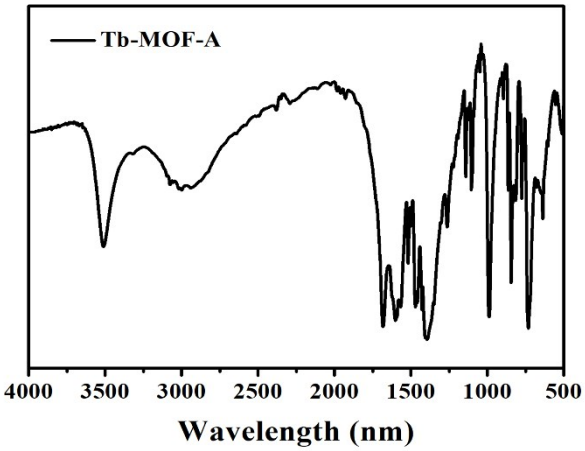

Figure S3. The IR spectra of Tb-MOF-A

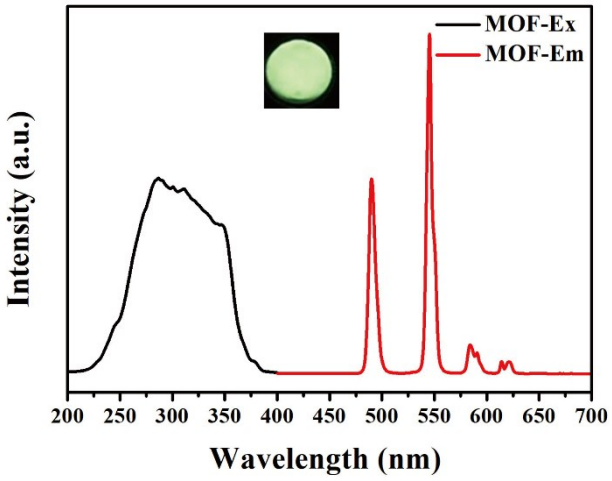

Figure S4. Excitation and emission spectra of free Tb-MOF-A.

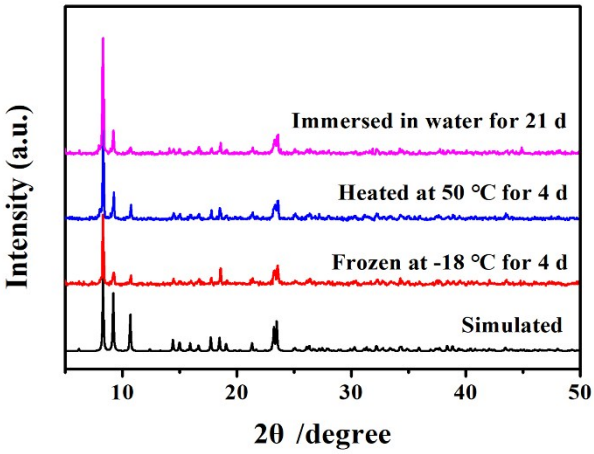

Figure S5. Simulated and experimental powder X-ray diffraction patterns (PXRD) patterns of Tb-MOF-A were immersed in water 21 days, frozen at -18 ℃, heated at 50 ℃ in water for 4 days.

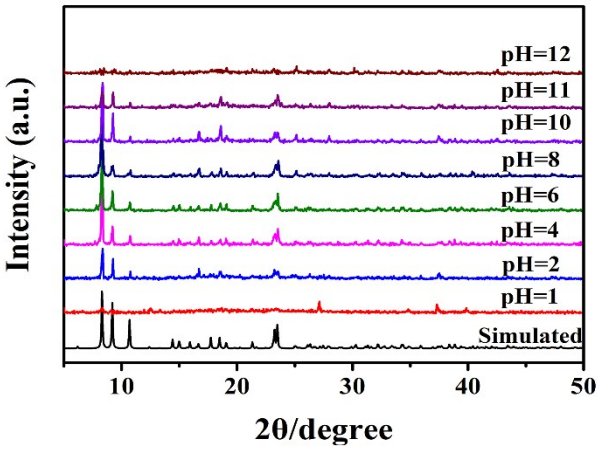

Figure S6. Simulated and experimental powder X-ray diffraction patterns (PXRD) patterns of Tb-MOF-A were treated by aqueous solutions with various pH values from 1 to 12.

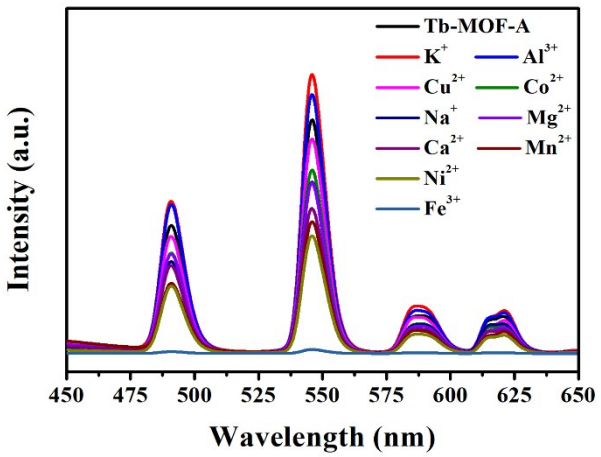

Figure S7. The emission spectra of **Tb-MOF-A** immersed in water of metal ions aqueous solutions.

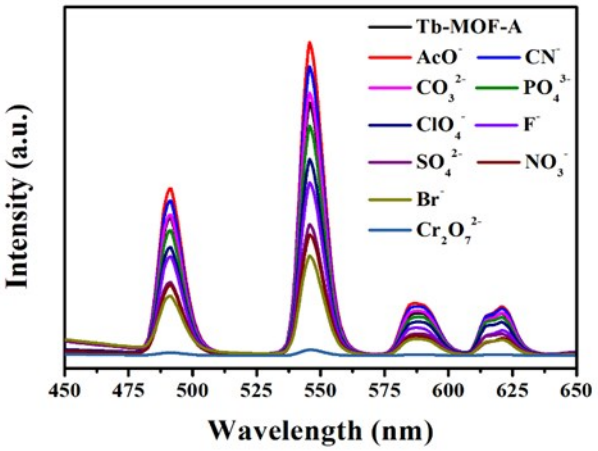

Figure S8. The emission spectra of Tb-MOF-A immersed in water of anions aqueous solutions.

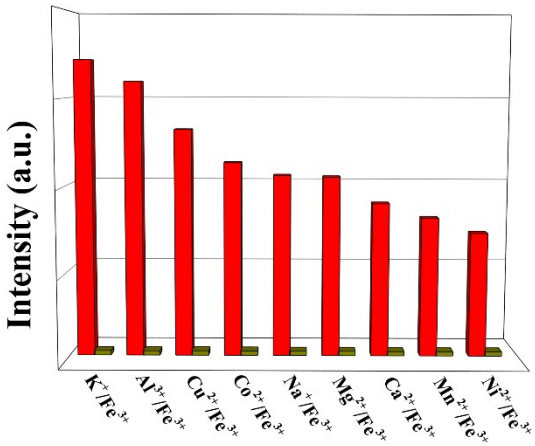

Figure S9. The competition experiments for the detection of Fe^{3+} ion in the presence of the interference metal cations.

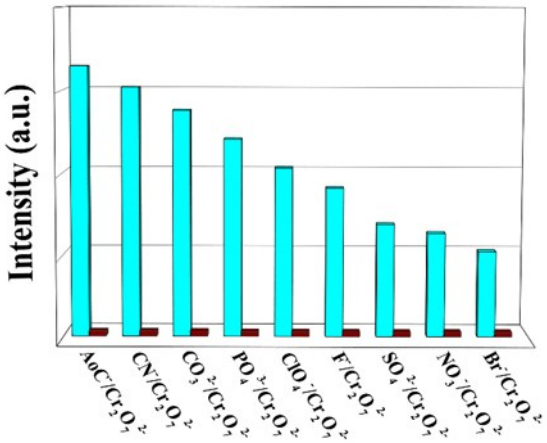

Figure S10. The competition experiments for the detection of $Cr_2O_7^{2-}$ ion in the presence of the interference anions.

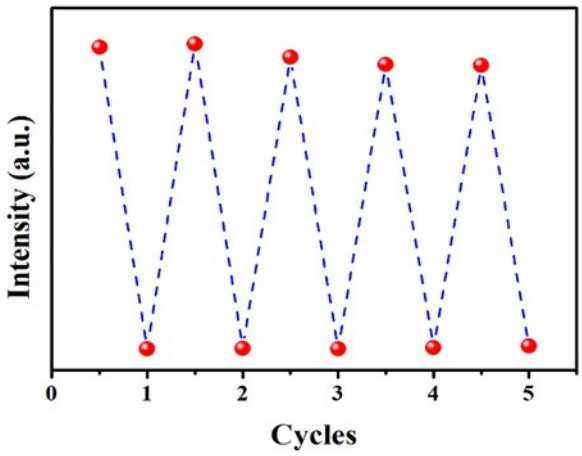

Figure S11. The quenching and recovery tests of **Tb-MOF-A** in water of Fe^{3+} ion.

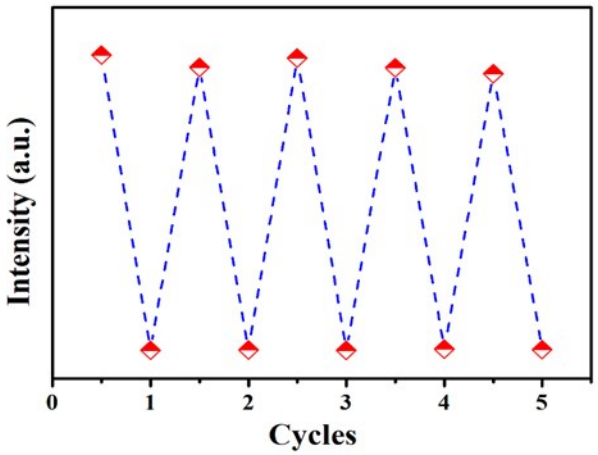

Figure S12. The quenching and recovery tests of **Tb-MOF-A** in water of $Cr_2O_7^{2-}$ ion.

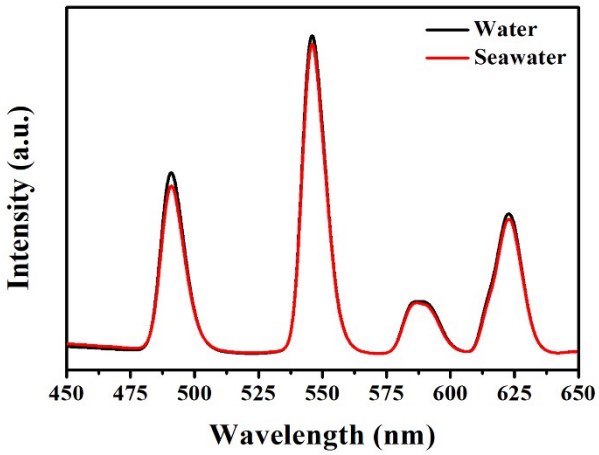

Figure S13. Luminescence spectra of Tb-MOF-A immersed in water (black)and in seawater (red) for 48 h

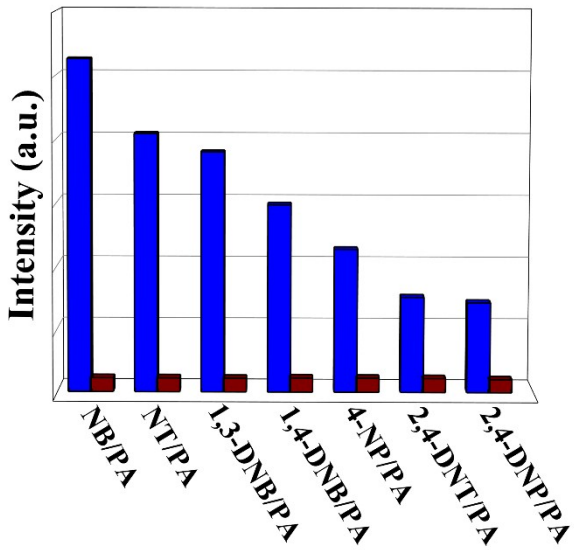

Figure S14. The competition experiments for the detection of PA in the presence of the interference nitro-explosives.

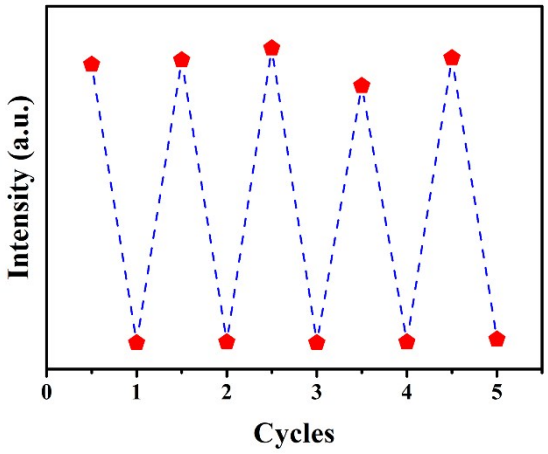

Figure S15. The quenching and recovery tests of **Tb-MOF-A** in seawater of PA.

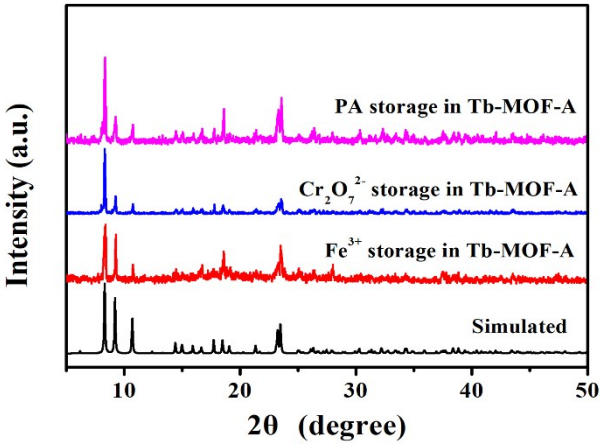

Figure S16. PXRD patterns of Tb-MOF-A after storage in Fe^{3+}, $Cr_2O_7^{2-}$, PA aqueous solutions.

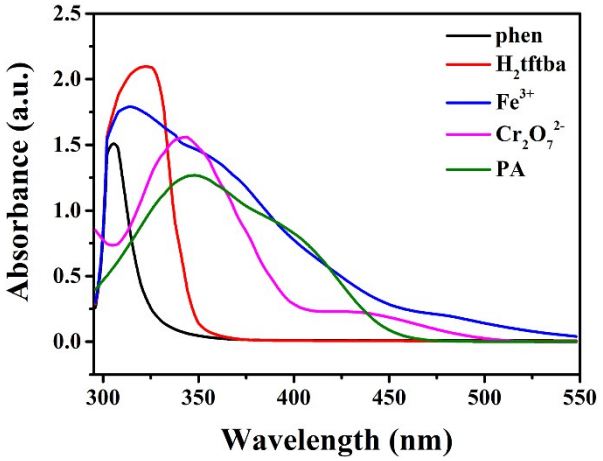

Figure S17. Spectral overlap between absorption spectra of the ligands of Tb-MOF-A and Fe^{3+}, $Cr_2O_7^{2-}$in water, PA in seawater.

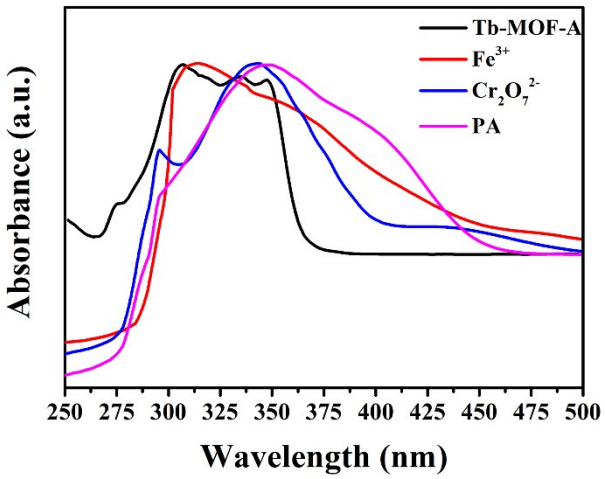

Figure S18. Spectral overlap between normalized excitation spectrum of Tb-MOF-A and normalized absorbance spectra of Fe^{3+}, $Cr_2O_7^{2-}$in water, PA in seawater.

Table S3. Comparison the Ksv of Tb-MOF-A towards Fe^{3+}, $Cr_2O_7^{2-}$ ions and PA with other materials.

Materials	analytes	solvent	$K_{SV}(M^{-1})$	Ref.
Tb-MOF-A	Fe^{3+}	H_2O	4.043×10^4	This work
Eu_4L_3	Fe^{3+}	DMF	2.942×10^3	2
L-N	Fe^{3+}	H_2O	7.93×10^3	3
L-F	Fe^{3+}	H_2O	1.39×10^3	3
$[Tb_4(L)_6(H_2O)_8]$	Fe^{3+}	H_2O	1.88×10^4	5
Eu-MOF	Fe^{3+}	H_2O	2.028×10^4	13
ZJU-109	Fe^{3+}	H_2O	5.641×10^4	14
$[Ln(Hpta)(C_2O_4)]\cdot3H_2O$	Fe^{3+}	H_2O	1.22×10^4	15
MOF-808-Tb	Fe^{3+}	H_2O	3.12×10^4	16
RhB@MOF	Fe^{3+}	H_2O	3.259×10^4	20
Tb-MOF-A	$Cr_2O_7^{2-}$	H_2O	2.857×10^4	This work
Eu_4L_3	$Cr_2O_7^{2-}$	DMF	1.526×10^3	2
$\{[Eu(L)(H_2O)_2]\cdot5H_2O\}_n$	$Cr_2O_7^{2-}$	H_2O	1.36×10^3	4
$[Tb_4(L)_6(H_2O)_8]$	$Cr_2O_7^{2-}$	H_2O	4.1×10^3	5
Eu-MOF	$Cr_2O_7^{2-}$	H_2O	1.141×10^4	13
$[Ln(Hpta)(C_2O_4)]\cdot3H_2O$	$Cr_2O_7^{2-}$	H_2O	1.02×10^4	15
NU-1000	$Cr_2O_7^{2-}$	H_2O	1.34×10^4	17
$[Cd_3(cpota)_2(phen)_3]_n\cdot5nH_2O$	$Cr_2O_7^{2-}$	H_2O	6.9×10^3	18
BUT-39	$Cr_2O_7^{2-}$	H_2O	1.57×10^4	19
Tb-MOF-A	PA	Seawater	5.890×10^4	This work
Eu_4L_3	PA	DMF	2.001×10^3	2
JLU-MOF48	PA	DMF	1.0×10^5	6
[Cd(L)(m-BDC)]	PA	DMF	4.67×10^4	7
$[Eu_2(ppda)_2(npdc)(H_2O)]\cdot H_2O$	PA	H_2O	3.44×10^5	8
TMU-5	PA	H_2O	3.5×10^4	9

Tb:Eu@MOF (5:1)	PA	DMF	1.414×10^5	10
$[Cd(NDC)_{0.5}(PCA)]\cdot G_x$	PA	H_2O	3.5×10^4	11
Bio-MOF-1	PA	DMF	4.5×10^4	12
GdL	PA	H_2O	4.48×10^4	21

Supplementary references

(1) S. L. C. Ferreira, H. C. dos Santos, M. S. Fernandes and M. S. de Carvalho, *J. Anal. At. Spectrom*., 2002, **17**, 115.

(2) W. Liu, X. Huang, C. Xu, C.Y. Chen, L. Z. Yang, W. Dou, W. M. Chen, H. Yang and W. S. Liu, *Chem. Eur. J.,* 2016, **22**, 18769-18772.

(3) W. W, N. Gong, H. Yin, B. Zhang, P. Guo, Bo Liu and Y. Y Wang, *Inorg. Chem.,* 2019, **58**, 10295-10303.

(4) P. F. Zhang, G. P. Yang, G. P. Li, F. Yang, W. Ni Liu, J. Y Li and Y. Y Wang, *Inorg. Chem.,* 2019, **58**, 13969-13978.

(5) X. N. Wang, J. L. Li, C. G. Jiang, P. Hu, B. Li, T. L Zhang and H. C Zhou, *Chem. Commun.,* 2018, **54**, 13271-13274.

(6) J. T Li, X. L Luo, Y. Zhou, L.R. Zhang, Q. S Huo and Y. L. Liu, *Cryst. Growth Des.,* 2018, **18**, 1857-1863.

(7) X. Du Zhang, J. A. Hua, J. H. Guo, Y. Zhao and W. Yin Sun, *J. Mater. Chem. C,* 2018, **6**, 12623-12630.

(8) Z. Y Zhan, X. Y Liang, X. L Zhang, Y. J Jia and M. Hu, *Dalton Trans.*, 2019, **48**, 1786-1794.

(9) M. Bagheri, M. Y. Masoomi, A. Morsali and A. Schoedel, *ACS Appl. Mater. Interfaces,* 2016, **8**, 21472-21479.

(10) X. F. Qiao, Y. B. Han, D. Tian, Z. C. Yang, J. L. Li and S. T. Zhao, *Sensors & Actuators: B. Chemical,* 2019, **286**, 1-8.

(11) S. S. Nagarkar, B. Joarder, A. K. Chaudhari, S. Mukherjee, S. K. Ghosh, *Angew. Chem., 2013,* **125**, 2953-2957.

(12) B. Joarder, A. V. Desai, P. Samanta, S. Mukherjee, S. K. Ghosh, *Chem. A Eur. J.,* 2015, **21**, 965-969.

(13) Y. H. Yu, M. Y. Fan , Q. Liu , Z. M. Su, X. Li, Q. Q. Pan, X. L. Hu, *Inorg. Chem.,* 2020, **59**, 2005-2010.

(14) Y. J. Cui, D. Yue, Y. K. Huang, J. Zhang, Z. Y. Wang, D. R. Yang and G. D. Qian, *Chem. Commun.*, 2019, **55**, 11231-11234.

(15) L. J Duan, C. C Zhang, P. P. Cen, X. Y. Jin, C. Liang, J. H. Yang and X. Y. Liu, *CrystEngComm*, 2020, **22**, 1695-1704.

(16) J. Zhang, S. B. Peh, J. Wang, Y. Du, S. Xi, J. Dong, A. Karmakar, Y. Wang, Y. Ying and D. Zhao*, Chem. Commun.*, 2019, **55**, 4727-4730.

(17) Z. J. Lin, H. Q. Zheng, H. Y. Zheng, L. P. Lin, Q. Xin, R. Cao, *Inorg. Chem.,* 2017, **56**, 14178-14188.

(18) S. Li, L. Lu, M. Zhu, C. Yuan, S. Feng, *Sens. Actuators, B*, 2018, **258**, 970-980.

(19) T. He, Y.Z. Zhang, X. J. Kong, J. M Yu, X. L. Lv, Y. F. Wu, Z. J. Guo and J. R. Li, *ACS Appl. Mater. Interfaces,* 2018, **10**, 16650-16659.

(20) L. Guo, Y. Liu, R. M Kong, G. Chen, Z. Liu, F. L. Qu, L. Xia and W. H. Tan, *Anal. Chem.,* 2019, **91**, 12453-12460

(21) L. Li, J. H Cheng, Z. P. Liu, L. Song, Y. J. You, X. H. Zhou and W. Huang, *ACS Appl. Mater.*

Interfaces, 2018, **10,** 44109-44115.